THE ASTROPHYSICAL JOURNAL, 166:465–481, 1971 June 15

ON THE DENSITY-WAVE THEORY OF GALACTIC SPIRALS

III. COMPARISONS WITH EXTERNAL GALAXIES

FRANK H. SHU, ROBERT V. STACHNIK, AND JONATHAN C. YOST
State University of New York at Stony Brook
Received 1970 August 13; revised 1971 February 4

ABSTRACT

We undertake a semiempirical study of the spiral patterns of three model galaxies constructed from the observed rotation curves of M33, M51, and M81. Consistent with the proposal that density waves are initiated in the outer regions of a galaxy, we find a good fit to result for the observed spiral structure if we choose a pattern speed equal to the rotation speed where the distribution of H II regions is seen to end. The circumferential bands containing the most prominent H II regions are located in qualitative agreement with a mechanism in which star formation is triggered by spiral galactic shocks. A suggestion is made for M51 for the coexistence of short and long trailing waves traveling with the same pattern speed.

I. INTRODUCTION

The winding dilemma associated with spiral tubes of matter in a field of differential rotation has led many workers, starting with B. Lindblad (1963 and earlier papers), to regard the principal arms of a spiral galaxy as the compression zones of a density wave. Indeed, recent studies (see review by Lin 1970) show that several large-scale observable features in our own Galaxy receive a comprehensive explanation in terms of a density wave that has a quasi-stationary spiral structure.

a) Objectives of the Present Paper

Several workers (Toomre 1969; Kalnajs 1970; Lin 1970; Lynden-Bell 1970; Miller, Prendergast, and Quirk 1970; Contopoulos 1970; Shu 1970*a*, *b*, hereinafter called Papers I and II, respectively) have commented recently on the possible *origin* and *development* of extensive spiral structure in normal spiral galaxies. Whether or not one adheres to any of their views, the theory of density waves, *with the pattern speed* Ω_p *regarded as a free parameter*, can help greatly in interpreting observations of external galaxies. In this spirit, we have included a sufficiently detailed account of the computational techniques to allow the application of the theory as a working tool.

b) Test of Lin's Proposal

As an illustration of this application, we adopt a semiempirical approach to test one aspect of Lin's (1970) proposal. Our approach is semiempirical in that we have not included the effects of boundary conditions in what may be regarded as a difficult and perhaps nonlinear eigenvalue problem; instead, we have determined the one crucial parameter of the theory Ω_p by the following line of reasoning.

If Lin is correct and density waves are initiated by gravitational clumping in the outer regions of spiral galaxies (see also Goldreich and Lynden-Bell 1965; Julian and Toomre 1966), then the resulting pattern speed is approximately equal to the rotation speed of the outermost H II region (Paper II). The corotation radius lies slightly outside the outermost H II region if star formation is initiated only by the mechanism of spiral galactic shocks (W. W. Roberts 1969), but it coincides with the H II region if the clumping of interstellar gas itself leads to star formation.

The spiral pattern associated with our own Galaxy appears to satisfy the above criterion (cf. Lin, Yuan, and Shu 1969). It is of interest to see whether the criterion is satisfied by external galaxies as well.

The test, then, is whether a theoretical pattern computed with a pattern speed estimated from the determination of the corotation radius provides a good fit to the observed spiral structure in the interior. This test is meaningful because the calculation of a spiral pattern is sensitive to the determination of the pattern speed but not to the details of the equilibrium model adopted (cf. § VI).

The normal spiral galaxies M33, M51, and M81 are selected for a first study because (*a*) the two-armed "grand design" of each galaxy is easily recognizable and (*b*) the kinematics of rotation of these galaxies span the familiar range from nearly solid-body rotation (M33) to nearly constant rotational velocity (M51 and M81). M51 is additionally interesting because one of its main spiral arms appears "aimed" at a close companion, NGC 5195. Thus, M51 provides an oft-quoted example in which close galactic companions may play an important role either in exciting or in disrupting spiral structure (cf. Pfleiderer 1963; Arp 1969; Toomre 1969; Toomre and Toomre 1970; see also § IV*e*).

II. CONSTRUCTION OF EQUILIBRIUM MODELS

Before we can compute the properties of the spiral density waves which propagate in a galaxy, we must first construct an equilibrium model. For simplicity, we shall consider only the stars; the inclusion of a small amount of gas (~10 percent) would not significantly modify our spiral-pattern determinations (Shu 1968). For our present purposes, then, we require self-consistent models of stellar disks which give not only the distribution of mass but also the distribution of velocities.

a) *Mass Models*

Methods for constructing static axisymmetric mass models of galaxies from observed rotation curves are well known (Schmidt 1956, 1965; Burbidge, Burbidge, and Prendergast 1959; Brandt 1960; Toomre 1963). In our studies, we represent the disk population by one of Toomre's flat models and the central bulge (if any) by one or more inhomogeneous spheroids. (See Appendix for details.) The distance D used to convert angular positions to radii from the center of the galaxy is listed in Table 1. The precise determination of this quantity is, fortunately, not essential for the comparison of the theoretically derived pattern with the observed spiral structure since the computed pattern scales with the linear size adopted for the galaxy (see also § V).

b) *Distribution of Peculiar Velocities and Thickness of the Disk*

Given a mass model, the formalism used by Shu (1969) for completely flat disks is extended (along lines similar to that of Vandervoort 1970*a*) to compute the velocity distribution for a galaxy of finite but small thickness. The resulting model has at each

TABLE 1

INTEGRAL PROPERTIES OF THE GALAXIES M33, M51, AND M81

Galaxy (1)	Type (2)	D (Mpc) (3)	M ($10^{10}\ M_\odot$) (4)	J* ($M_\odot$ kpc km sec^{-1}) (5)	E* ($M_\odot$ km^2 sec^{-2}) (6)	EJ^2/G^2M^5 (7)	$M_{\rm H\,I}/M$ (8)
M33...	Sc	0.794	1.66	7.84×10^{12}	-6.69×10^{13}	−0.177	0.12
M51...	Sc	4.00	1.96	6.89×10^{12}	-1.99×10^{14}	−0.178	0.042
M81...	Sb	2.63	12.3	1.64×10^{14}	-3.44×10^{15}	−0.175	0.012

* Computed as if the disk were completely flat and in centrifugal equilibrium.

point a (modified) Schwarzschild distribution of peculiar velocities. Such a stellar disk has a mass distribution which varies in the vertical direction as $\operatorname{sech}^2(z/z_0)$. The parameter $z_0(\varpi)$ is the local scale height and is given in terms of the mean-square peculiar velocity $\langle c_z^2\rangle$ by

$$z_0 = \langle c_z^2\rangle/\pi G\sigma_0 \,, \tag{1}$$

where σ_0 is the local surface density.

c) The Velocity Dispersions

The velocity dispersions in the (modified) Schwarzschild distribution cannot be chosen arbitrarily but must satisfy the dynamical constraints of equilibrium and stability. Thus, the velocity dispersion $\langle c_\theta^2\rangle^{1/2}$ relative to $\langle c_\varpi^2\rangle^{1/2}$ is given by Lindblad's (1959) theory of small epicyclic motions. If we write κ and Ω for the rotational and epicyclic frequencies, Lindblad's theory gives

$$\langle c_\theta^2\rangle^{1/2}/\langle c_\varpi^2\rangle^{1/2} = \kappa/2\Omega \,, \tag{2a}$$

$$\kappa^2 = 4\Omega^2 + \varpi d\Omega^2/d\varpi \,. \tag{2b}$$

On the other hand, the ratio $Z_{\text{II}} = \langle c_z^2\rangle^{1/2}/\langle c_\varpi^2\rangle^{1/2}$ probably has the value unity in the central regions of spiral galaxies where a well-mixed state of equilibrium (Jeans 1922) can be expected to prevail. In the outer regions of a thin-disk galaxy, the decoupling of the motion perpendicular to the plane from those parallel to it (which depends on existence of a "third integral") can lead to values of Z_{II} substantially less than unity (e.g., $Z_{\text{II}} = 0.5$–0.6 in the solar neighborhood). In our models, Z_{II} decreases monotonically from unity at the galactic center to 0.5 at the outermost regions. The choice of the rate of decrease is arbitrary; fortunately, the computed spiral pattern is insensitive to this choice.

It remains, thus, to specify $\langle c_\varpi^2\rangle^{1/2}$ as a function of radius. The minimum value $\langle c_\varpi\rangle_{\min}^{1/2}$ is obtained by requiring that the stellar disk be stable against the Jeans instability for the rotating disk (cf. Toomre 1964, Fig. 5, for the case of a stellar disk of infinitesimal thickness). We have plotted in Figure 1 the results of extending Toomre's

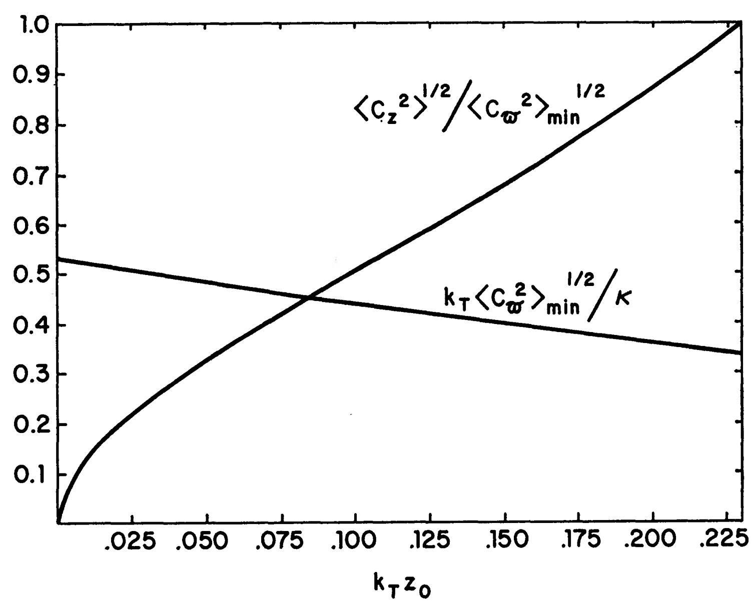

FIG. 1.—Criterion of marginal stability as a function of the dimensionless disk thickness $k_T z_0$

criterion to a stellar disk with given (local) thickness z_0. The results are most compactly stated in the dimensionless form where $k_T\langle c_\varpi^2\rangle_{\min}^{1/2}/\kappa$ and $\langle c_z^2\rangle^{1/2}/\langle c_\varpi^2\rangle_{\min}^{1/2}$ are plotted as a function of $k_T z_0$. The parameter k_T is the natural inverse-length scale associated with the rotation of a thin disk (Toomre 1964):

$$k_T = \kappa^2/2\pi G\sigma_0 . \tag{3}$$

As an illustration of the utility of Figure 1, suppose the solar neighborhood to possess just the minimum level of $\langle c_\varpi^2\rangle^{1/2}$ consistent with stability. Following Schmidt (1965), we adopt the value $\kappa = 32$ km sec^{-1} kpc^{-1}. We also adopt as reasonable estimates $\sigma_0 = 90\, M_\odot$ pc^{-2} and $z_0 = 300$ pc. These two estimates correspond to a volume density in the central plane equal to $\sigma_0/2z_0 = 0.15\, M_\odot$ pc^{-3}, i.e., Oort's (1965) limit. Using equation (3), we compute $k_T = 0.421$ kpc^{-1} and $k_T z_0 = 0.126$. From Figure 1, we now obtain $\langle c_z^2\rangle^{1/2}/\langle c_\varpi^2\rangle^{1/2} = 0.60$ and $\langle c_\varpi^2\rangle^{1/2} = 0.42\ (\kappa/k_T) = 32$ km sec^{-1}. The last two values are in good agreement with observations (cf. Delhaye 1965; see also Vandervoort 1970*c* for a treatment more elaborate than ours). A more realistic estimate, based on approximately 10 percent of the local surface density being in the form of interstellar gas with an "effective sonic speed" $a = 8$ km sec^{-1} would raise our estimate of $\langle c_\varpi^2\rangle_{\min}^{1/2}$ by about 3 km sec^{-1} (Shu 1968).

The apparent coincidence between the velocity dispersion actually present in the solar neighborhood and the minimum required for stability reinforces our conviction that the stability index $Q = \langle c_\varpi^2\rangle^{1/2}/\langle c_\varpi^2\rangle_{\min}^{1/2}$ is likely to have a value near unity throughout the interior of the disk, except possibly for the very central regions (cf. Shu 1969; see also Toomre 1964). For this reason and for simplicity, we adopt $Q = 1$ throughout the disk of our models.

III. LOCAL PROPERTIES OF SPIRAL DENSITY WAVES

The dispersion relation for spiral density waves has been derived in the WKBJ approximation for stellar disks of infinitesimal thickness by Lin (1966) and Lin and Shu (1966). The extension of this analysis to disks of finite thickness was undertaken by Shu (1968) and by Vandervoort (1970*b*). A second-order analysis giving the variation of the amplitude of the wave for a disk of infinitesimal thickness was considered in Paper II. In what follows, we shall use the notation of Paper II to put the results of these investigations in a form useful for our studies.

a) Dispersion Relation

For a stellar disk which possesses a (modified) Schwarzschild distribution of peculiar velocities, the dispersion relation giving the local wavenumber $k = \Phi'(\varpi)$, for given wave frequency ω, takes the form (Shu 1968; Vandervoort 1970*b*):

$$\frac{k_T}{|k|}(1-\nu^2) = \mathfrak{F}_\nu \mathfrak{Z} , \tag{4a}$$

$$\nu = (\omega - m\Omega)/\kappa = m(\Omega_p - \Omega)/\kappa , \tag{4b}$$

with $m = 2$ for two-armed spirals.

The functions $\mathfrak{F}_\nu$ and $\mathfrak{Z}$ are, respectively, the "reduction factors" due to the effects of velocity dispersion in the galactic plane and in the vertical direction. (For the functional form of $\mathfrak{F}_\nu$, see Lin *et al.* 1969.) In what follows, we use the form

$$\mathfrak{Z} = \frac{1}{1+|k|z_0} , \tag{5}$$

which is the "crude" approximation of Vandervoort (1970*b*). Numerically, it differs little from the "reduction factor due to thickness" introduced by Shu (1968). For $z_0 =$

0, $\mathfrak{J} = 1$, and the dispersion relation (4a) reduces to that given by Lin and Shu (1966) for a flat stellar disk.

The dispersion relation (4a) leads *formally* to an interesting degeneracy. For a given frequency ω and angular symmetry m, waves of two different scales arise because of the different roles played by rotation and "pressure" in opposing the force of self-gravity (Paper II, Fig. 1). Indeed, Lin's (1970) proposal for the origin of spiral structure relies on a coherent superposition of inwardly propagating short waves and outwardly propagating long waves to maintain a two-armed trailing spiral mode.

The existence of the *long* waves is speculative since the assumptions underlying the WKBJ approximation (e.g., the neglect of azimuthal forces for nonaxisymmetric disturbances) break down for very long waves. Pending further theoretical analysis, we consider the existence of long waves only as an interesting working hypothesis.

b) Amplitude of the Wave

For a disk of infinitesimal thickness, the variation with radius of the amplitude of the wave has been derived in Paper II (see also Toomre 1969). There has as yet been no rigorous extension of this second-order WKBJ analysis for a disk of finite thickness. A heuristic and qualitatively correct result is given below. Call $g = (g_\varpi^2 + g_\theta^2)^{1/2}$ the mass-weighted average of the amplitude of the spiral gravitational field and express it as a fraction F of the mean gravitational field $\varpi\Omega^2$; then

$$F = g/\varpi\Omega^2 = \text{constant} \times (k^2\varpi^2 + m^2)^{1/2}|\varpi\mathfrak{R}_\nu|^{-1/2}/\varpi\Omega^2\,, \tag{6a}$$

$$\mathfrak{R}_\nu = \left[-1 + \frac{\partial \ln}{\partial \ln k}(\mathfrak{F}_\nu \mathfrak{J})\right]. \tag{6b}$$

It is easy to verify that these equations reduce to the correct limit for vanishing disk thickness (cf. eq. [59] of Paper II).

The amplitude relation given above implies that the action density $\mathfrak{A}$, the energy density $\mathcal{E} = \omega\mathfrak{A}$, and the angular-momentum density $\mathcal{J} = m\mathfrak{A}$ of the wave are positive for the outer regions of a galaxy where $\Omega < \Omega_p$ but negative for the inner regions where $\Omega > \Omega_p$ (cf. Toomre 1969; Paper II). Thus, provided that wave energy can be exchanged across the corotation circle $\Omega = \Omega_p$, and provided that the global wave energy is zero, the square of the wave amplitude (which is locally proportional to $\mathfrak{A}$) can grow spontaneously without violating the global conservation of energy and angular momentum (Kalnajs 1970). If the corotation circle is located sufficiently inward (i.e., if Ω_p is sufficiently high), sufficient material may exist beyond the corotation circle to allow the outer regions to play as important a dynamical role as the inner regions. In this case, the overstability mechanism of Kalnajs may lead to the spontaneous excitation of spiral density waves. From our analysis (§§ IV*a*, V, VI), this is a definite possibility for M33.

c) Numerical Reliability of the WKBJ Approximation

For the WKBJ approximation to be applicable, the parameters

$$\delta_1 = (|k|\varpi)^{-1}\,, \quad \delta_2 = \left|\frac{1}{2k\varpi}\frac{d \ln \mathfrak{R}_\nu}{d \ln \varpi}\right|\,, \quad \delta_3 = \exp[-(\varpi - \varpi_L)^2/2\varepsilon^2\varpi^2]\,, \tag{7}$$

must be small compared with unity. In the above, ϖ_L is the radius of a Lindblad resonance ring (if one exists) and ε is the dimensionless parameter $\langle c_\varpi^2\rangle^{1/2}/\varpi\kappa$.

The requirement $\delta_1 \ll 1$ is the general condition for the validity of the asymptotic expansion. Clearly, this requirement cannot be satisfied (*a*) if the waves reach the central regions so that ϖ is small or (*b*) if the waves are very long so that $|k|$ is small. The criterion $\delta_2 \ll 1$ guarantees the coefficients of the terms of $O(\delta_1)$ in the asymptotic expansion to be small in comparison with those of $O(1)$ (more specifically, that the magnitude of the second term in the brackets of eq. [11] in Paper II [generalized to incorporate the effects of finite thickness] be small compared with the first). This criterion is violated, for example, near the corotation radius where the amplitude of the self-consistent spiral gravitational field is no longer slowly varying in comparison with the phase. The condition $\delta_3 \ll 1$ breaks down when we are within a distance $O(\varepsilon\varpi)$ of a Lindblad resonance (Paper II, eq. [42]).

For definiteness, we adopt the following practical criteria for numerical reliability:

$$\delta_1\,, \quad \delta_2\,, \quad \delta_3 < 0.3\,. \tag{8}$$

In practice, the parameters δ_1, δ_2, δ_3 are usually much smaller than 0.3 throughout most of the range of the computed pattern for short waves.

d) Rate of Star Formation

According to the shock calculations of W. W. Roberts (1969), the degree of gas compression, along a streamline of average radius ϖ, depends on four parameters: a, k, Ω_p, and F. If the two-component model of the interstellar medium (Field, Goldsmith, and Habing 1969; Spitzer and Scott 1969) is adopted, a is unlikely to be very different from the sound speed associated with the intercloud phase ($\sim$7–12 km sec^{-1} for a wide range of densities).[1]

The dependence of the solution for the gas flow on k and Ω_p is essentially through the combination

$$w_{\perp 0} = m\varpi(\Omega - \Omega_p)/(k^2\varpi^2 + m^2)^{1/2}\,, \tag{9}$$

which represents the component of the unperturbed gas velocity perpendicular to the wave front. If $w_{\perp 0} \sim a$, the maximum compression felt by the gas may be greatly enhanced by the development of galactic shocks induced by the presence of the spiral gravitational field. The degree of enhancement depends on the magnitude of F.

IV. RESULTS

a) Rotation Curves and Equilibrium Models

The curves marked $\varpi\Omega$ in Figures 2*a*, 2*b*, and 2*c* represent our fits of the observational data on rotation curves for M33, M51, and M81 (see Appendix for details). Our model for M33 is nearly in solid-body rotation for much of the interior of the disk, whereas our models for M51 and M81 show considerable differential rotation. Apart from size, the main difference between M51 and M81 seems to be the amounts of matter in gas relative to that in stars (see Table 1). The solid and dotted curves in Figure 2*b* give two examples of plausible fits for the observational data on M51. We adopt the solid curve for pattern calculations and use the dotted curve to illustrate the errors which arise from observational uncertainties.

The curves marked σ in Figures 2*a* and 2*b* show the surface densities corresponding to our fits of the rotation curves for M33 and M81. The corresponding curves for the two models of M51 are shown separately in Figure 2*d*. In contrast with the distribution of mass in M33, those in M51 and M81 are sharply peaked toward the galactic center. The smooth distribution for M33 seems to be in accord with the distribution of Population II and old Population I stars indicated by the composite photograph of Walker (Lequeux 1969, Plate X).

Figure 3 shows for M33 the adopted dispersion velocities and scale height z_0 as functions of distance from the galactic center. The disk thickness z_0 is different from that adopted originally to compute the rotation curve in Figure 2*a*. In principle, we should adjust that rotation curve if we retain the same projected mass density σ. However,

[1] In Roberts's calculations, a represents the turbulent dispersion speed of the gas = speed of random motions of the interstellar clouds $\sim$10 km sec^{-1}.

1971ApJ...166..465S

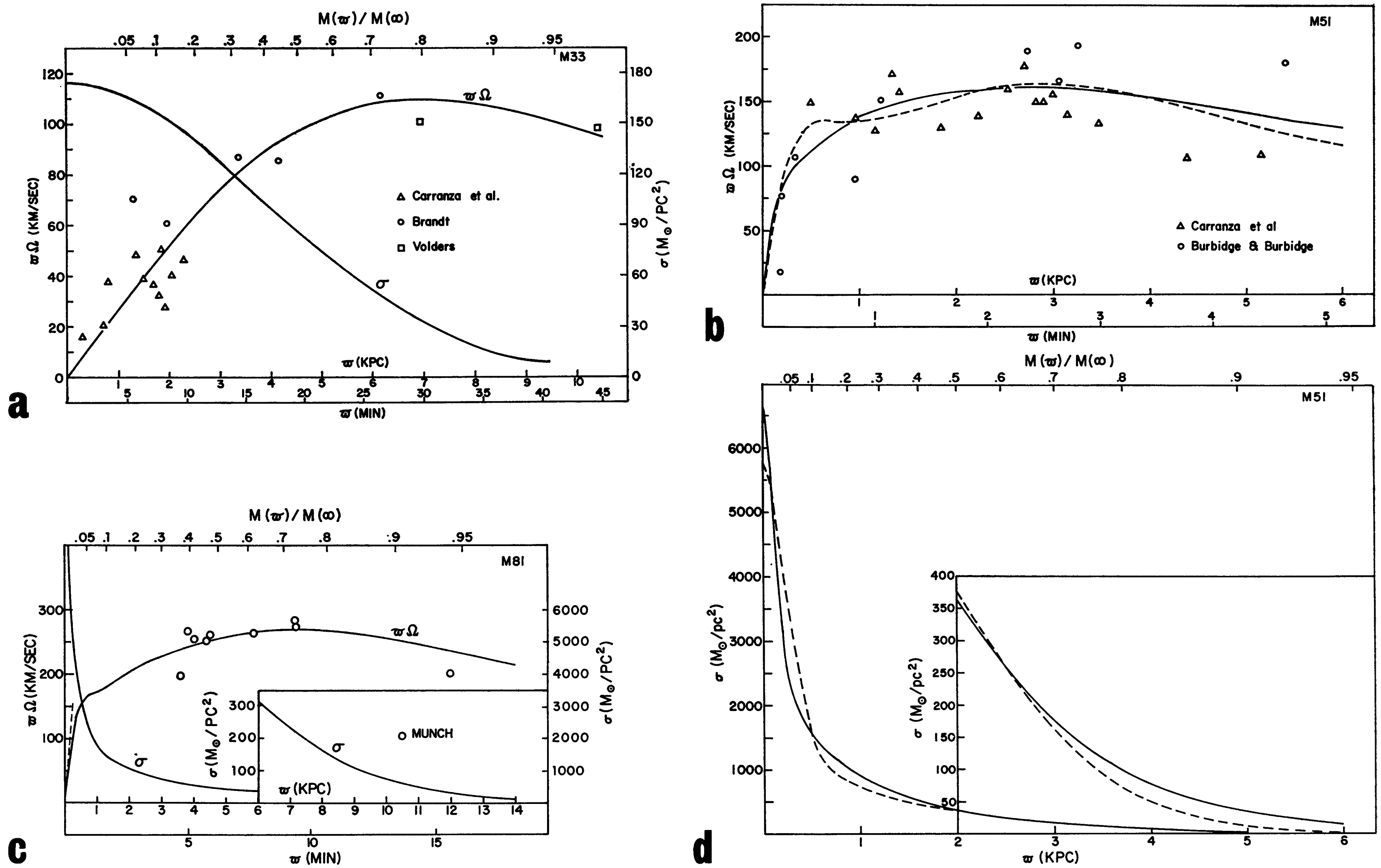

FIG. 2.—Rotation curves and surface densities of M33, M51, and M81. Curves marked $\varpi\Omega$ represent the circular velocities; those marked σ, the surface densities of our models. Each tick at the top of the figures marks off the fraction of the total mass contained in a cylinder interior to the tick.

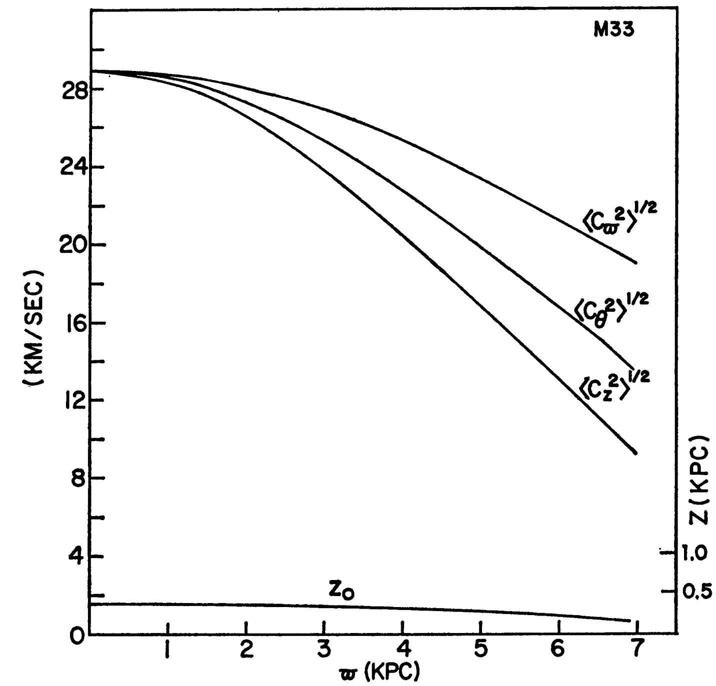

FIG. 3.—The dispersion velocities and scale height adopted for M33. The dispersion velocities are calculated on the assumption that the level of dispersion present is barely sufficient for the suppression of the Jeans instability. The scale height z_0 is associated with the balance between the gravitational potential and the random motions in the vertical direction.

since the adjustment required is $O(z_0^2/\varpi^2)$ and is negligible everywhere except in the very central regions, we ignore the slight modifications required. The dispersion velocities and scale heights for M51 and M81 are computed in a similar fashion but are not displayed here.

b) Determination of Pattern Speeds

Figures 4*a*, 4*b*, and 4*c* show the run of the rotation parameters Ω, κ, $\Omega \pm \frac{1}{2}\kappa$. Two-armed spiral waves can propagate only in the range where a horizontal line drawn at height Ω_p lies above $\Omega - \frac{1}{2}\kappa$ and below $\Omega + \frac{1}{2}\kappa$. However, if Lin (1970) is correct, only the region where $\Omega - \frac{1}{2}\kappa < \Omega_p < \Omega$ shows an *organized* spiral pattern.

The location of the outermost H II region in our algorithm gives the corotation radius, i.e., where $\Omega = \Omega_p$. This determines Ω_p to be given approximately by 16 km sec^{-1} kpc^{-1} for M33 and 21.5 km sec^{-1} kpc^{-1} for M81—corresponding to corotation at 6.8 and 11.2 kpc, respectively. In view of the likely disruption of the outermost parts of M51 by the companion NGC 5195, this method may not give a reliable estimate of the corotation radius of M51. Under these circumstances, we arbitrarily adopt $\Omega_p = 33$ km sec^{-1} kpc^{-1} (corresponding to corotation at 4.5 kpc) as a value considered not inconsistent with Lin's proposal.

Because Ω is fairly constant over the disk of M33, the curve $\Omega - \frac{1}{2}\kappa$ is very flat. Hence, ingoing spiral waves excited with a pattern speed of 16 km sec^{-1} kpc^{-1} can penetrate into the very center of the galaxy. This can be expected to be a general feature of galaxies which possess no prominent concentrations of mass toward the galactic center. In contrast, for our choices of the pattern speeds, the ingoing spiral waves in M51 and M81 would encounter barriers provided by the existence of inner Lindblad resonances.

Related to the previous comment is a dynamical tendency for galaxies like M33 to

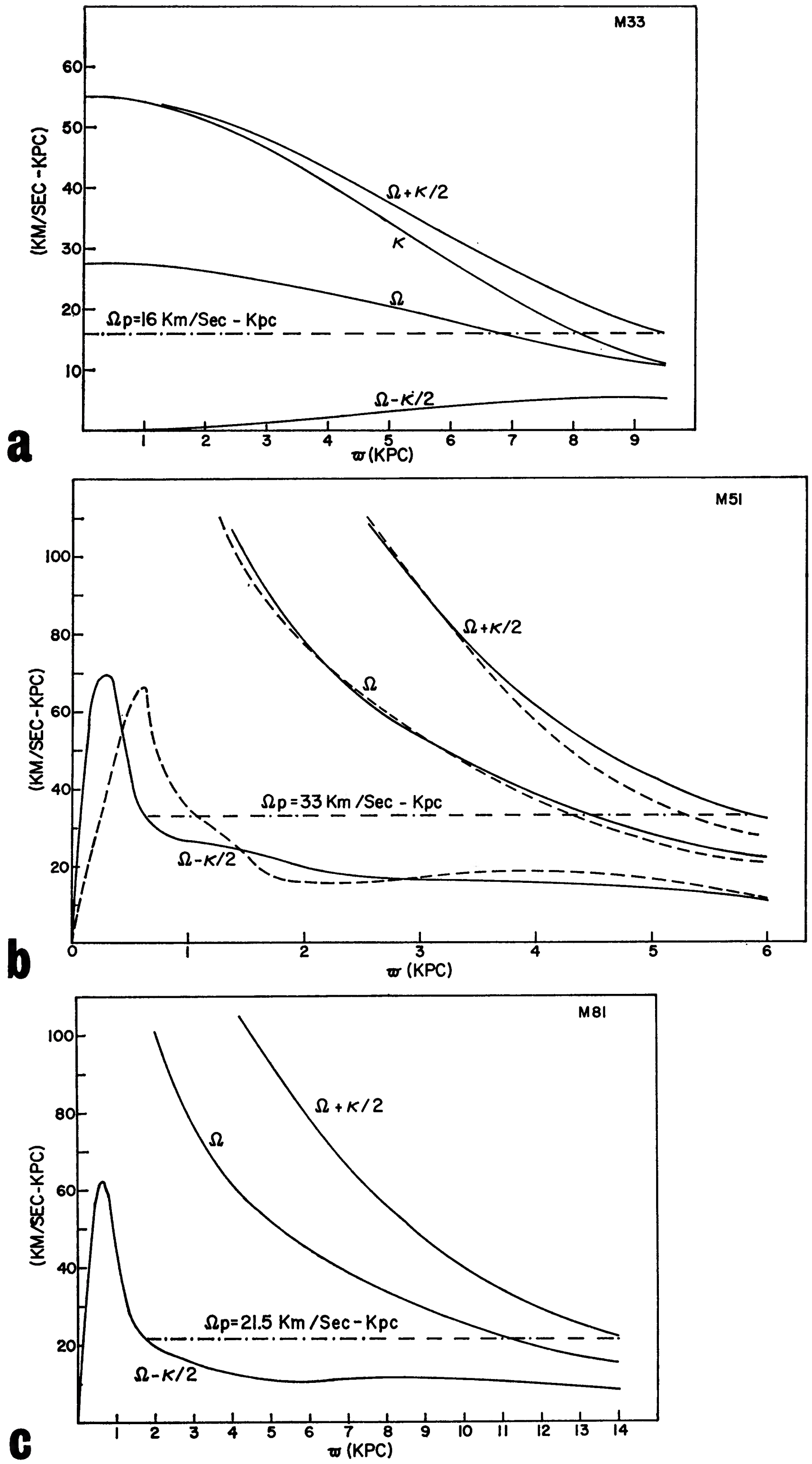

FIG. 4.—Angular speeds of rotation Ω, epicyclic frequencies κ, and the combinations $\Omega \pm \frac{1}{2}\kappa$ according to the mass models for M33, M51, and M81.

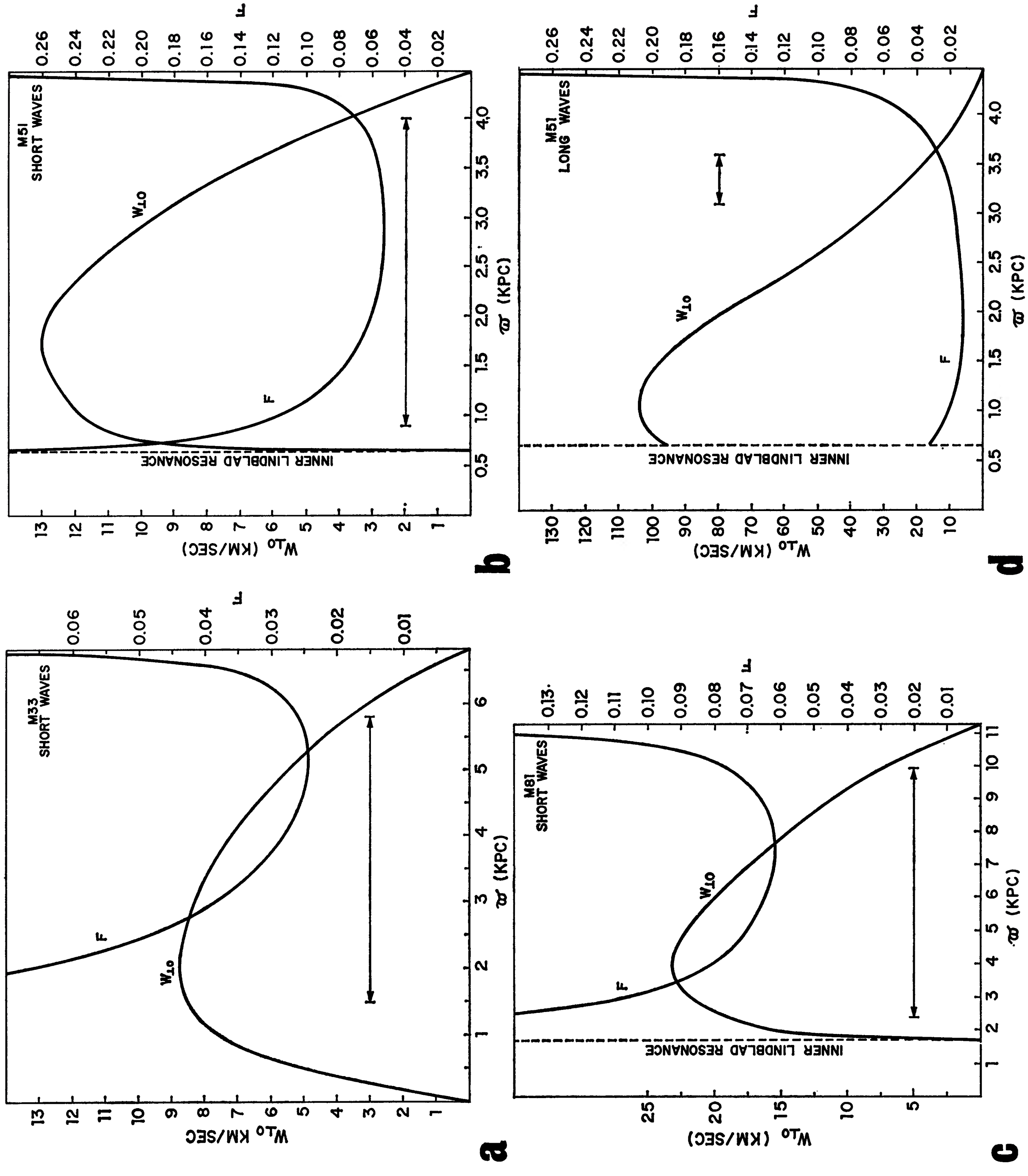
M51
SHORT WAVES
$W_{\perp o}$ (KM/SEC)
F
ϖ (KPC)
INNER LINDBLAD RESONANCE
b
M33
SHORT WAVES
$W_{\perp o}$ KM/SEC
a
M51
LONG WAVES
d
M81
SHORT WAVES
c

have more open spiral arms. The waves in such galaxies are likely to be everywhere far from (Lindblad) resonance with the consequence that the dispersion relation will never give very short wavelength scales for the self-sustained waves.

c) *Spiral Patterns*

The solid curves of Figures 5*a*, 5*b*, and 5*c* (Plates 1, 2, and 3) show the spiral patterns computed for the short waves as an overlay, when properly scaled and tilted, on the photographs of M33, M51, and M81 contained in *The Hubble Atlas of Galaxies* (Sandage 1961). The computed patterns seem to give satisfactory fits for the primary spiral features observed in these galaxies. In particular, the waves in M33 can propagate into the galactic center and result in a barlike structure there, whereas in M51 and M81 they end as an increasingly tighter spiral around the inner Lindblad resonance ring.[2] We caution, however, that our analysis is incomplete since conditions near resonances and at the boundaries are not adequately treated. Note also the two-headed horizontal arrows in Figures 6*a*, 6*b*, and 6*c* which give the ranges over which the pattern calculations are considered numerically reliable.

d) *Rates of Star Formation*

Plotted in Figures 6*a*, 6*b*, and 6*c* as functions of ϖ are F and $w_{\perp 0}$ (see eqs. [6a] and [9]) associated with the short spiral waves in M33, M51, and M81. Reference to the shock calculations of W. W. Roberts (1969) for our own Galaxy would lead us to expect a noticeable decrease, for $\varpi \gtrsim 3$ kpc in M33, in the rate of star formation by the mechanism of triggering by spiral galactic shocks. This occurs because both F and $w_{\perp 0}$ decrease rapidly as one goes outward from 3 kpc. This conclusion is in qualitative agreement with our visual impression of the observed spiral structure in M33.

In contrast, we would expect significant star formation to extend relatively farther out toward the corotation radius in M51 and M81, because $w_{\perp 0}$ maintains a value consistently closer to the assumed gaseous sonic speed a ($\sim$7–12 km sec^{-1}). This expectation is borne out by M51 but not by M81. We conclude that appreciable star formation extends only to $\sim$6 kpc in M81 because of the overall deficiency in interstellar gas. Thus, greater gas compression may be required intrinsically to trigger star formation in M81 today.

e) *Additional Comments on M51*

i) *Disruption by NGC 5195*

Toomre and Toomre (1970; see also Pfleiderer 1963) have shown the outermost portions of a disk galaxy to suffer impressive gravitational disruptions (with the formation of transient "intergalactic bridges" and "counter-jets") during the close passage of another galaxy. The disruption is very considerable unless the orbit of the companion either has a high inclination with respect to the principal plane of the target galaxy or is in a retrograde sense with respect to the rotation of the target galaxy.[3] The difference of

[2] Indeed, our adoption of the particular model for M81 was influenced by the location of an apparently circular arc of dust marking a radius $\sim$1.7 kpc.

[3] In this regard we remark that while Toomre's calculations refer to material particles, there is little distinction between density waves and and material arms near the corotation circle.

FIG. 6.—The unperturbed velocity components $w_{\perp 0}$ and the relative amplitudes F of the spiral gravitational field: (*a*) for short waves propagating with $\Omega_p = 16$ km sec^{-1} kpc^{-1} in M33, (*b*) for short waves propagating with $\Omega_p = 33$ km sec^{-1} kpc^{-1} in M51, (*c*) for short waves propagating with $\Omega_p = 21.5$ km sec^{-1} kpc^{-1} in M81, and (*d*) for *long* waves propagating with $\Omega_p = 33$ km sec^{-1} kpc^{-1} in M51. The right-hand borders of the abscissa correspond to the corotation radii. The horizontal two-headed arrows indicate the ranges over which the calculations are considered numerically reliable. The absolute scales for F are arbitrary, but in (*d*) they can be compared relative to those in (*b*) provided that total reflection of short waves into long waves (and vice versa) occurs.

FIG. 5.—The spiral patterns of M33, M51, and M81; comparison of theory and observations. (*a*) The theoretical pattern is drawn out to the corotation radius of M33 at 6.8 kpc.

SHU *et al.* (*see* page 475)

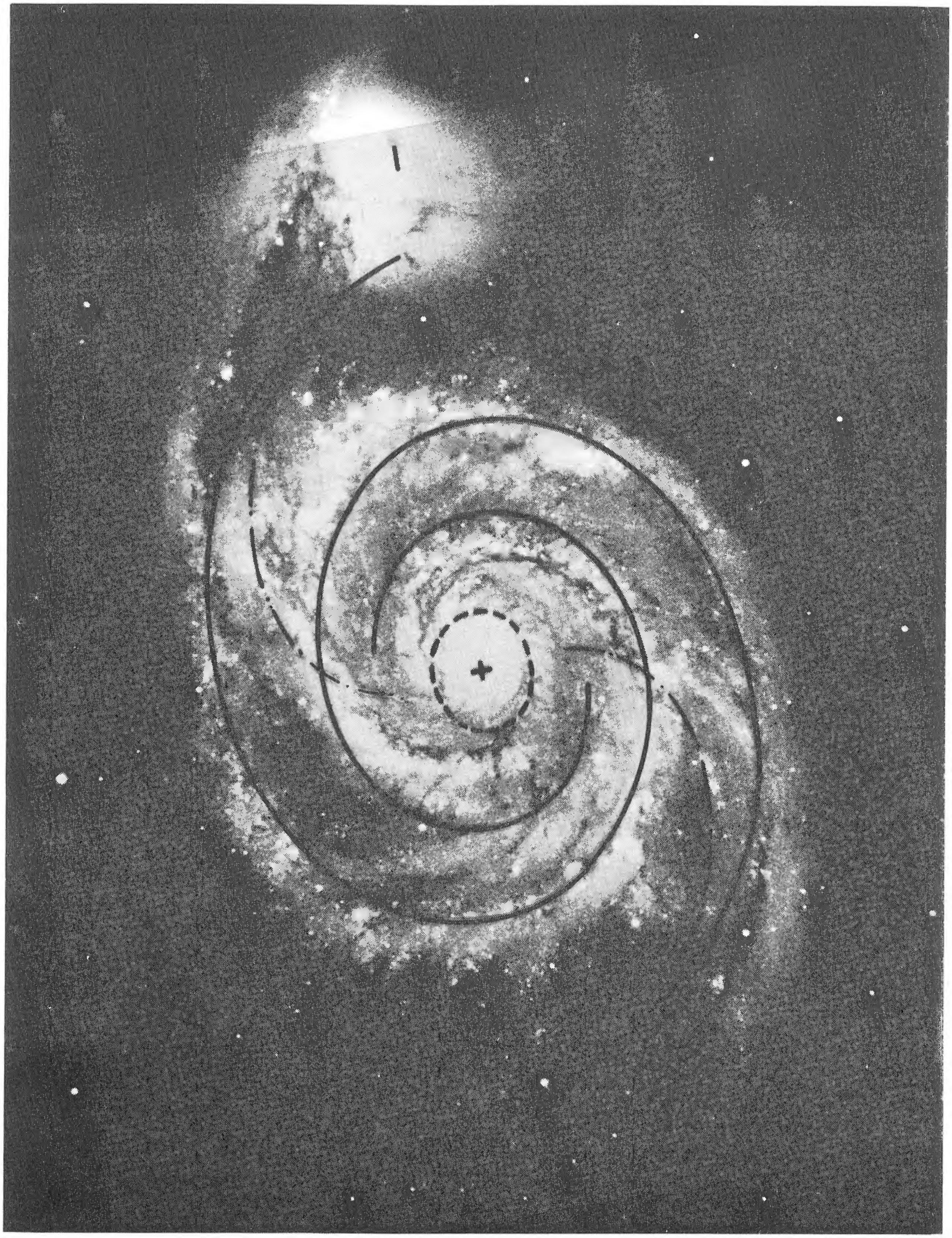

FIG. 5.—The spiral patterns of M33, M51, and M81; comparison of theory and observations. (*b*) Dotted ring denotes the location of the inner Lindblad resonance in M51 at 0.65 kpc. *Solid curve*, short-wave pattern; *dash-dot curve*, long-wave pattern.

SHU *et al*. (*see* page 475)

1971ApJ...166..465S

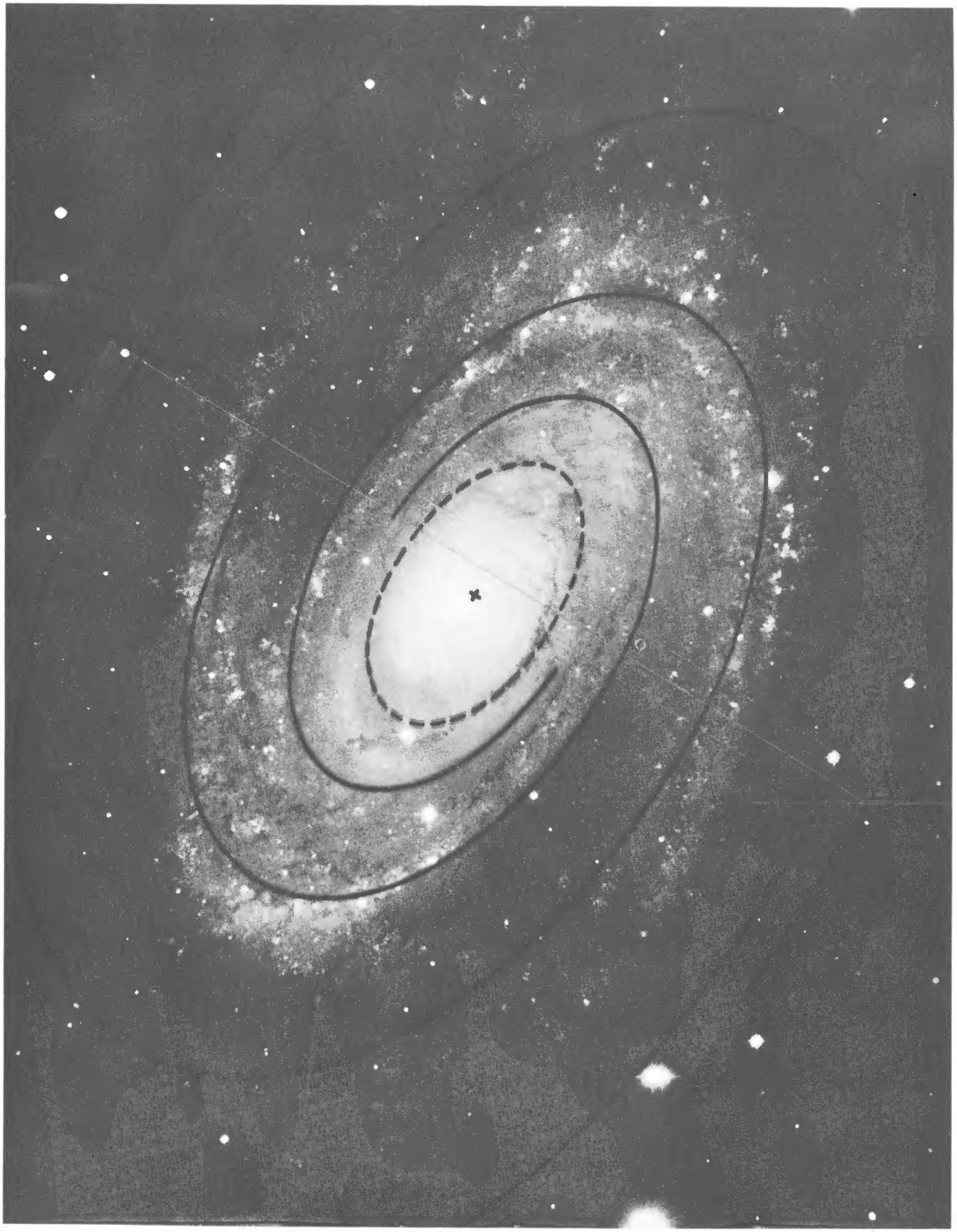

FIG. 5.—The spiral patterns of M33, M51, and M81; comparison of theory and observations. (*c*) Dotted ring denotes location of the inner Lindblad resonance in M81 at 1.7 kpc. The extension of the theoretical pattern to the corotation radius at 11.2 kpc lies beyond the edges of the plate.

SHU *et al.* (*see* page 475)

132 km sec^{-1} kpc^{-1} in the velocities of recession of NGC 5195 and M51 (Burbidge and Burbidge 1964) suggests the likelihood of a high-inclination orbit for NGC 5195 (cf. Carranza, Crillon, and Monnet 1969). Thus, aside from a "stretching" of the outermost parts of M51 toward and away from NGC 5195, we believe the disruption of M51 to be relatively minor. With this proviso, the agreement between the computed short-wave pattern and the observed spiral structure seems to be satisfactory.

ii) *Long Waves and the Branching of the Main Spiral Arms*

An interesting feature of the observed spiral structure in M51 is the occurrence of a branching of the two main spiral arms (Sandage 1961) at (nearly) *diametrically opposite points* for $\varpi \simeq 2.3$ kpc. The two branches make (nearly) the *same* characteristic angle of intersection with the main arms, an observation which suggests that the branches possess large-scale organization and are also part of the "grand design" rather than sheared material irregularities.

Our interpretation is to identify the two branches with the long waves invoked by Lin (1970) to feed back the inwardly propagating signal of the short waves. The location of the crests of the long waves is drawn as the dash-dot curve in Figure 5*b*.[4] Our interpretation is supported by the presence of two distinct dust lanes associated with the spiral arm which "bridges" to the companion galaxy.

The very large unperturbed Mach numbers coupled with the relatively weak spiral field F associated with the long waves in the interior (see Fig. 6*d*) makes unlikely the development of periodic galactic shocks. Rather, the flow probably remains hypersonic with respect to the long waves along the whole length of the stream tube, and the gas compression is relatively small. Our conjecture is that this low gas compression is usually insufficient to trigger star formation unless the gas has been "suitably prepared" upstream by passage through a short-wave arm. This conjecture would explain why the *luminous* branches are initiated at the intersection of the wave fronts and continue outward from there.

A cautionary note is needed, however. Figure 6*d* also shows the criteria δ_1, $\delta_2 < 0.3$ to be satisfied only over 3.1 kpc $< \varpi <$ 3.6 kpc. Hence, the agreement between the theoretical location of the long waves and the observed location of the branches may be illusory.

Finally, we note that the two main arms of M81 also seem to branch at $\varpi \simeq 4$ kpc. Unfortunately, a formal calculation of the long-wave pattern here is virtually meaningless since the criteria δ_1, $\delta_2 < 0.3$ are satisfied only for 8.0 kpc $< \varpi <$ 9.2 kpc.

V. INTEGRAL PROPERTIES

With a view to establishing a quantitative basis for the classification of normal spiral galaxies, we list in Table 1 the integral properties of the galaxies M33, M51, and M81. Column (7) gives the only dimensionless quantity which can be formed from the total energy E, the total angular momentum J, the total mass M, and the universal gravitational constant $G = 4.298 \times 10^{-6}$ (km sec^{-1})^2 kpc/$M_\odot$. Column (8) gives, as a fraction of the total mass, the mass in the form of H I (M. S. Roberts 1969) after normalization to the distance scales and total masses adopted for our studies. If the real distance, for a given galaxy, is cD rather than D, then the real mass, angular momentum, energy, and fractional gas content are cM, c^2J, cE, and $cM_{\rm H\,I}/M$ rather than M, J, E,

[4] The long-wave pattern is computed with its phase at corotation matched with that of the short wave (otherwise the repeated reflections of the waves would not lead to reinforcement). To help make our case, we take the liberty of rotating by 10° toward the companion galaxy, the line of nodes advocated by the Burbidges (1964). In view of the likely distortion produced by NGC 5195 and inasmuch as the Burbidges quote a probable error of $\pm 10°$ for their determination of the position angle of the semi-major axis of M51, this freedom of action is not considered excessive.

and M_{HI}/M. The dimensionless constant in column (7) is, of course, unaffected by a change in scale.

From Table 1, the value EJ^2/G^2M^5 is seen to remain nearly invariant from galaxy to galaxy.[5] Although this invariance may have evolutionary implications, it is also possible that the combination EJ^2/M^5 is *very insensitive* to the details of the near-centrifugal equilibrium as long as extreme conditions are not realized. This possibility is reminiscent of the behavior found by Mestel (1963) for the *detailed distribution* of angular momentum in various galactic models. (The [near] invariance found by Mestel is even more striking since it involves a function rather than a scalar.)

For reference, let us also note that the fractional masses contained beyond the corotation circle are, respectively, 22, 13, and 7 percent in the models adopted for M33, M51, and M81. These numbers should not be regarded as being more than merely indicative since considerable extrapolation of the observational data is required to produce them.

VI. DISCUSSION

a) Uncertainties of the Analysis

A primary uncertainty of our analysis arises because the observations do not allow the construction of a unique model for the galaxy. A case in point is given for M51 in Figures 2*b*, 2*d*, and 4*b*. Table 2 shows various parameters associated with the two models of M51 when $\Omega_p = 33$ km sec^{-1} kpc^{-1} and when $\Omega_p = 43$ km sec^{-1} kpc^{-1}. From this table, we conclude:

1. Except for the location (but not the *existence*) of the inner Lindblad resonance, the main features of the spiral pattern, *for given* Ω_p, are not sensitive to the details of the model adopted. In particular, the tilt angle $i = \arctan (m/|k|\varpi)$ is essentially determined by the major features of the basic model.

2. The pattern calculation *is sensitive* to changes in Ω_p (i.e., to the location of the corotation radius). A 30 percent increase in Ω_p—from 33 to 43 km sec^{-1} kpc^{-1}—for M51 results in a pattern whose tilt angle i is increased by roughly 30 percent and whose radii at corotation and the outer Lindblad resonance are decreased by roughly 20 percent (because the rotation curve is nearly Keplerian at these distances).

Our computed patterns tend systematically to be somewhat too tight in comparison with the observed structures. Consequently, if our determinations of the pattern speeds are to be revised at all, they should probably be revised upward. Nevertheless, our determination of the pattern speeds (corotation radii) for M51 and M81 are probably not too low by more than ~30 percent (too large by more than ~20 percent). Otherwise,

TABLE 2

PARAMETERS OF SPIRAL PATTERNS FOR TWO MODELS OF M51

Pattern Speed Ω_p (km sec^{-1} kpc^{-1})	Model of M51	Radius (kpc)*			Inclination i	
		ILR	C	OLR	2.0 kpc	3.0 kpc
33........	Solid curve	0.65	4.5	5.9	8°1	9°0
	Dotted curve	1.1	4.4	5.4	8.3	7.9
43........	Solid curve	0.50	3.6	5.0	10.4	11.9
	Dotted curve	0.85	3.6	4.6	10.2	10.6

* ILR = inner Lindblad resonance, C = corotation, OLR = outer Lindblad resonance.

[5] The invariance does not arise, in an obvious manner, as a result of our model-fitting procedure since our models contain as many as eleven adjustable constants.

apart from difficulties with the tilt angles, even the entire principal range (from the inner to the outer Lindblad resonance) would not suffice to span the radial extent of the observed structure.

The situation for M33 is considerably less restrictive. From an analysis of the systematic variation in color of newly born stars as one cuts across a segment of the "southern arm" of M33, Dixon (1971) has suggested that corotation may occur near 3 kpc ($\Omega_p \simeq$ 25 km sec^{-1} kpc^{-1} in our model). Dixon's results are not necessarily in conflict with ours. The part of the "southern arm" he discusses ($\varpi \gtrsim 3$ kpc) has no analogue on the opposite side of the galaxy and, hence, needs not be a direct continuation of the two-armed structure in the interior.

On the other hand, if corotation does occur near 3 kpc, the tilt angles for $\varpi \lesssim 3$ kpc should be $\sim$1.5 times larger than those computed for corotation at 6.8 kpc. Such a pattern calculation based on equation (4a) would, admittedly, have little numerical reliability. It is possible that only a more refined theoretical treatment can settle this point. In this regard, M33 makes an ideal candidate for further theoretical study—the complications of an inner Lindblad resonance are absent, and, moreover, the existing optical and radio observational data are extensive.

b) Conclusions

The concept of the initiation of density waves by the Jeans instability in the outer regions of normal spiral galaxies (Lin 1970) is consistent with our study of the spiral structures of M33, M51, and M81. We have not shown that Lin's proposal is the only one consistent with the observations. In particular, an overstability mechanism such as that of Kalnajs (1970) could well be driving the spiral pattern of M33.

Much work remains to be done. We have analyzed the spiral patterns of only three external galaxies. Clearly, considerable extension is needed if we are to put the classification of normal spirals by their optical forms on a quantitative physical basis. Serious unsettled questions remain concerning the theory of the origin of density waves (Paper I). In terms of physical processes, we also urgently need to understand the detailed mechanisms by which clouds and stars form in an interstellar medium which is subjected to periodic compressions and decompressions.

We acknowledge with pleasure many fruitful discussions with Drs. W. Gebel, A. J. Kalnajs, C. C. Lin, P. O. Lindblad, M. S. Roberts, S. E. Strom, R. B. Tully, and P. O. Vandervoort. This work was supported in part by the National Science Foundation grant GP 13061.

APPENDIX

I. MASS MODELS OF TOOMRE

The surface density and the square of the angular speed of rotation of the (n_{T})th mass model in the sequence considered by Toomre (1963) can be written in the expanded form (below, $n_{\mathrm{T}} = n + 1$)

$$\sigma_0(\varpi) = \frac{B^2 A}{2\pi G} \frac{(2n+1)!}{(n!2^n)^2} \eta^{n+3/2}, \quad \Omega^2(\varpi) = B^2 T_{n+1}(\eta) . \tag{A1}$$

In equation (A1), A and B are adjustable constants which have the dimensions of a length and an angular velocity. The variable η and the function $T_{n+1}(\eta)$ are given by

$$\eta = (1 + \varpi^2/A^2)^{-1}, \quad T_{n+1}(\eta) = \sum_{j=0}^{n} \frac{(2n-2j)!(2j+1)!}{[j!(n-j)!2^n]^2} \eta^{j+3/2} . \tag{A2}$$

II. SPHEROIDAL MASS MODELS

We also adopt a sequence of inhomogeneous spheroids of eccentricity e. If the variable a is defined by

$$a = [\varpi^2 + z^2/(1 - e^2)]^{1/2}\,, \tag{A3}$$

the volume density of the (n_s)th model in the sequence is taken to be of the form (below, $n_s = n$)

$$\begin{aligned} \rho(a) &= \frac{B^2(1 - a/A)^n}{4\pi G(1 - e^2)^{1/2}} \quad \text{for} \quad a \le A\,, \\ &= 0 \qquad\qquad\qquad\quad \text{for} \quad a \ge A\,. \end{aligned} \tag{A4}$$

In equation (A4), A and B are adjustable constants which have the dimensions of a length and an angular velocity. The surface density and the square of the angular speed of rotation (in the plane $z = 0$) which correspond to the above mass distribution are given by (cf. Schmidt 1965)

$$\sigma_0(\varpi) = \frac{B^2\varpi}{2\pi G}\sum_{j=0}^{n}\binom{n}{j} Q_{j+2}(\xi)\left(-\frac{\varpi}{A}\right)^j\,, \tag{A5a}$$

$$\Omega^2(\varpi) = B^2\sum_{j=0}^{n}\binom{n}{j}\frac{P_{j+3}(\eta)}{e^{j+3}}\left(-\frac{\varpi}{A}\right)^j\,. \tag{A5b}$$

The variables ξ and η are given by

$$\begin{aligned} \xi &= A/\varpi\,, \quad \eta = e\,, \qquad\quad \text{for} \quad \varpi \le A\,; \\ \xi &= 1\,, \qquad \eta = eA/\varpi \quad \text{for} \quad \varpi \ge A\,, \end{aligned} \tag{A6}$$

whereas the functions $Q_{j+1}(\xi)$ and $P_{j+1}(\eta)$ are obtained from the integrals

$$Q_{j+1}(\xi) = \int_0^{\text{arc cosh }\xi} \cosh^j \gamma d\gamma\,, \qquad P_{j+1}(\eta) = \int_0^{\text{arc sin }\eta} \sin^j \beta d\beta\,. \tag{A7}$$

The latter have the recursion relations (for $j = 2, 3, \ldots$)

$$Q_{j+1}(\xi) = \frac{1}{j}[\xi^{j-1}(\xi^2 - 1)^{1/2} + (j - 1)Q_{j-1}(\xi)]\,, \tag{A8a}$$

$$P_{j+1}(\eta) = \frac{1}{j}[-\eta^{j-1}(1 - \eta^2)^{1/2} + (j - 1)P_{j-1}(\eta)]\,, \tag{A8b}$$

$$Q_1(\xi) = \text{arc cosh }\xi\,, \qquad Q_2(\xi) = (\xi^2 - 1)^{1/2}\,, \tag{A8c}$$

$$P_1(\eta) = \text{arc sin }\eta\,, \qquad P_2(\eta) = 1 - (1 - \eta^2)^{1/2}\,. \tag{A8d}$$

III. THE EPICYCLIC FREQUENCY AND THE SUPERPOSITION OF MASS MODELS

For Toomre's mass models and for the spheroidal mass models with $n_s \ge 2$, the square of the epicyclic frequency (as defined by eq. [2b]) is everywhere differentiable (i.e., "smooth") and positive. For $n_s = 1$, κ^2 is continuous (but not differentiable) at $\varpi = A$, and can, for e sufficiently close to unity, be negative for ϖ near A. The case $n_s = 0$ corresponds to a uniformly rotating spheroid.

When the mass distributions of two or more models are superposed linearly, the gravitational forces are superposed linearly. Consequently, Ω^2 and κ^2 are also superposed linearly.

For our fits of M51 and M81, two spheroid models are combined with a Toomre model. The length scales A are adjusted to fit certain features of the rotation curve, e.g., the radius of the turnover point, the radius of the velocity maximum, etc. Then, the constants B^2 are adjusted to provide a least-squares-error fit for $\varpi^2\Omega^2$. For M81, we include a fit for the angular velocity of the central regions.

For our fit of M33, a single Toomre model is used. The constants A and B^2 are adjusted simultaneously to yield a least-squares-error fit for $\varpi^2\Omega^2$. Table 3 gives the values of the parameters adopted for the mass models of M33, M51, and M81.

IV. REDUCTION OF THE DATA

a) M33

The circles in Figure 2*a* represent rotational-velocity determinations by Brandt (1965) from Hα emission; the triangles, those by Carranza *et al.* (1967) from Hα emission; the squares, those by Volders (1959) from 21-cm emission. To reduce scatter, Brandt's measurements are combined so that each circle represents a total statistical weight of approximately 2 (Brandt 1965, Table III). The individual measurements of Carranza *et al.* are combined by threes. The consideration of the more detailed features available from Carranza *et al.* (1968) would not lead to significant differences in the determination of a (mean) rotation curve. Their extensive observations should, however, prove useful for a study of the velocity field associated with the spiral structure of M33. The radio observations of Volders are critical for the determination of the turnover point. The beamwidth used for these observations is about 30′. Clearly, finer-resolution studies would be extremely useful.

b) M51

The circles in Figure 2*b* represent rotational- velocity determinations by Burbidge and Burbidge (1964); the triangles, those by Carranza *et al.* (1969). Each circle is taken directly from Figure 2 of the Burbidges' paper and represents, on the average, the mean of five individual measurements. Their measurements for regions near the galactic center are not included since we do not discuss here the role of noncircular motions. Each triangle represents the mean of four individual measurements of Carranza *et al.* for the southern half of M51. (We have followed these authors in not using the data from the northern half of the galaxy.)

TABLE 3

PARAMETERS FOR THE MASS MODELS OF M33, M51, AND M81

	Galaxy			
Model and Parameter	M33	M51 (Dotted Curves)	M51 (Solid Curves)	M81
Toomre:				
n_T	50	50	3	5
A (kpc)	38.75	17.00	4.200	13.00
B (km sec^{-1} kpc^{-1})	3.905	12.29	50.55	27.71
(First) spheroid:				
n_s	...	2	5	5
e	...	0.8718	0.8718	0.8718
A (kpc)	...	0.7000	0.6500	1.400
B (km sec^{-1} kpc^{-1})	...	692.2	1036	875.0
(Second) spheroid:				
n_s	...	2	5	5
e	...	0.9800	0.9800	0.9800
A (kpc)	...	1.500	2.800	6.000
B (km sec^{-1} kpc^{-1})	...	213.0	295.9	194.5

c) *M81*

The circles in Figure 2*c* represent rotational-velocity measurements of H II regions by Münch (1959). The dotted line gives his determination, from nuclear emission lines, of the angular velocity of rotation for the central regions. The relatively smaller number of emission knots in M81 leads, understandably, to less extensive data than for the Sc galaxies M33 and M51.

REFERENCES

Arp, H. 1969, *Sky and Tel.*, **38**, 385.
Brandt, J. C. 1960, *Ap. J.*, **131**, 293.
———. 1965, *M.N.R.A.S.*, **129**, 309.
Burbidge, E. M., and Burbidge, G. R. 1964, *Ap. J* , **140**, 1445.
Burbidge, E. M , Burbidge, G R., and Prendergast, K. H 1959, *Ap. J* , **130**, 739.
Carranza, G., Courtes, G , Georgelin, Y., and Monnet, G 1967, *C.R* , **264**, 191
Carranza, G., Courtes, G., Georgelin, Y., Monnet, G., and Pourcelot, A. 1968, *Ann. d'ap.*, **31**, 63.
Carranza, G , Crillon, R , and Monnet, G 1969, *Astr and Ap* , **1**, 479
Contopoulos, G 1970, *Ap. J.*, **160**, 113.
Delhaye, J. 1965, in *Galactic Structure*, ed. A. Blaauw and M. Schmidt (Chicago: University of Chicago Press), p. 61.
Dixon, M. E. 1971, *Ap J.*, **164**, 411.
Field, G. B., Goldsmith, D. W., and Habing, H. J. 1969, *Ap. J.* (*Letters*), **155**, L149.
Goldreich, P., and Lynden-Bell, D. 1965, *M.N R A S.*, **130**, 125.
Jeans, J. H. 1922, *M.N R.A.S* , **82**, 123.
Julian, W. H., and Toomre, A. 1966, *Ap J* , **146**, 810.
Kalnajs, A. J. 1970, in *The Spiral Structure of Our Galaxy*, ed W. Becker and G Contopoulos (Dordrecht: D. Reidel Publishing Co.), p. 314.
Lequeux, J. 1969, *Structure and Evolution of Galaxies* (New York: Gordon & Breach).
Lin, C. C. 1966, *SIAM J. Appl. Math.*, **14**, 876.
———. 1970, in *The Spiral Structure of Our Galaxy*, ed. W. Becker and G Contopoulos (Dordrecht: D. Reidel Publishing Co.), p. 373.
Lin, C. C., and Shu, F. H. 1966, *Proc. Nat. Acad. Sci* , **55**, 229.
Lin, C. C., Yuan, C., and Shu, F. H. 1969, *Ap. J.*, **155**, 721.
Lindblad, B. 1959, *Hdb. d. Phys.*, **53**, 21
———. 1963, *Stockholm Obs. Ann.*, **22**, 3.
Lynden-Bell, D. 1970, in *The Spiral Structure of Our Galaxy*, ed W. Becker and G. Contopoulos (Dordrecht: D. Reidel Publishing Co.), p. 331.
Mestel, L. 1963, *M.N.R.A.S.*, **126**, 553.
Miller, R. H., Prendergast, K. H , and Quirk, W J. 1970, *Ap. J.*, **161**, 903.
Münch, G. 1959, *Pub. A.S.P.*, **71**, 101.
Oort, J. H. 1965, in *Galactic Structure*, ed. A. Blaauw and M. Schmidt (Chicago: University of Chicago Press), p. 457.
Pfleiderer, J. 1963, *Zs. f. Ap.*, **58**, 12.
Roberts, M. S. 1969, *A.J.*, **74**, 859.
Roberts, W. W. 1969, *Ap. J.*, **158**, 123.
Sandage, A. 1961, *The Hubble Atlas of Galaxies* (Washington D.C.: Carnegie Institution of Washington).
Schmidt, M. 1956, *B.A N* , **13**, 15.
———. 1965, in *Galactic Structure*, ed. A. Blaauw and M. Schmidt (Chicago: University of Chicago Press), p 513.
Shu, F. H. 1968, unpublished Ph D. thesis, Harvard University.
———. 1969, *Ap. J.*, **158**, 505.
———. 1970*a*, *ibid.*, **160**, 89 (Paper I).
———. 1970*b*, *ibid.*, p. 99 (Paper II).
Spitzer, L., and Scott, E H. 1969, *Ap. J.*, **158**, 161.
Toomre, A. 1963, *Ap. J.*, **138**, 385.
———. 1964, *ibid.*, **139**, 1217
———. 1969, *ibid.*, **158**, 899.
Toomre, A , and Toomre, J. 1970, *Bull. A.A.S.*, **2**, 350.
Vandervoort, P. O. 1970*a*, *Ap. J.*, **161**, 67.
———. 1970*b*, *ibid* , p. 87.
———. 1970*c*, Dept. Astr. and Ap., Univ. of Chicago, Preprint No. 37
Volders, L. 1959, *B.A.N.*, **14**, 323.